


Simulation of diffusio-phoretic motion of colloidal particle suppressed by bound solutes within adsorption shell

Jiachen Wei

To cite this article: Jiachen Wei (2020): Simulation of diffusio-phoretic motion of colloidal particle suppressed by bound solutes within adsorption shell, Molecular Physics, DOI: [10.1080/00268976.2020.1718226](https://doi.org/10.1080/00268976.2020.1718226)



To link to this article: <https://doi.org/10.1080/00268976.2020.1718226>

 View supplementary material 

 Published online: 26 Jan 2020.

 Submit your article to this journal 

 Article views: 3

 View related articles 

 View Crossmark data 

RESEARCH ARTICLE



Simulation of diffusio-phoretic motion of colloidal particle suppressed by bound solutes within adsorption shell

Jiachen Wei^{a,b}

^aInstitute of Mechanics, Chinese Academy of Sciences, Beijing, People's Republic of China; ^bDepartment of Chemistry, University of Cambridge, Cambridge, UK

ABSTRACT

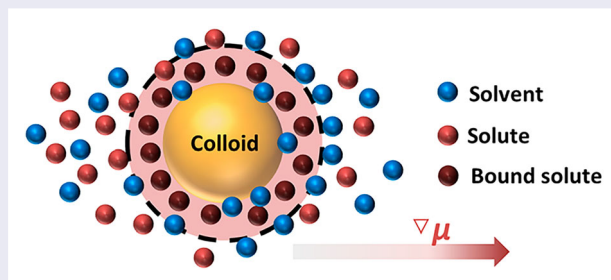
Colloidal particle submerged in a non-equilibrium fluid with a concentration gradient of solutes experiences diffusio-phoresis. Such directional transport originates from the driving forces that exert on the fluid in a microscopic boundary layer surrounding the colloid. Based on a simple model of spherical colloid fixed in a concentration gradient of solutes, molecular dynamics simulations are performed to determine the interaction parameters that maximise the diffusio-phoretic mobility, which cannot be properly measured by conventional continuum theory. The diffusio-phoretic mobility is found to depend non-monotonically on the strength of the interaction between the colloid and solutes, due to the presence of bound solutes within adsorption shell that cannot contribute to diffusio-phoresis. The results also show that the phoretic mobility depends sensitively on the density of solutes in bulk, due to the uneven distribution of excess particles surrounding the colloid at a microscopic level. The simulations suggest that diffusio-phoresis may in principle be applied to the selective transport, separation and purification for colloidal systems. By substituting the spherical colloid with other realistic macromolecules, the model could provide results that are quantitatively comparable with experiments.

ARTICLE HISTORY

Received 6 November 2019
Accepted 9 January 2020

KEYWORDS

Diffusio-phoresis; molecular dynamics; colloid; phoretic transport





1. Introduction

The phoretic effects are a class of transport phenomena induced by gradients of chemical potential [1–8], temperature [9–22], charge [23–28], etc. Diffusio-phoresis describes the spontaneous migration in a gradient of solute concentration [29–32], which plays important roles in separation science [33–37], pattern formation [5,32,38,39] and even dynamics in a living cell [40].

The migration of colloidal particles by phoresis has long been described by continuum models and hydrodynamics [2,8,25,30,41,42], which provide an adequate explanation for the experimental results. For

diffusio-phoresis with short-ranged interactions, however, the Stokesian hydrodynamics no longer holds near the fluid-colloid interface, as it fails to picture the effects of density and enthalpy fluctuations that emerge at microscopic level [43,44]. Inspired by the previous works on diffusio- and thermo-osmosis [45,46], in this article molecular dynamics simulations are implemented to describe the local structure and dynamics of the fluid. The gradient of solute concentration can be generated either explicitly with fixed source and sink of solute particles [14,44,47,48], or implicitly by applying external forces on each particle [45,46].

CONTACT Jiachen Wei ✉ weijiachen@nm.imech.ac.cn  Institute of Mechanics, Chinese Academy of Sciences, Beijing 100190, People's Republic of China; Department of Chemistry, University of Cambridge, Cambridge CB21EW, UK.

 Supplemental data for this article can be accessed here. <https://doi.org/10.1080/00268976.2020.1718226>

Based on these techniques of non-equilibrium molecular simulations, results for the diffusio-phoretic motion of a colloidal particle in a very weak gradient of solute concentration are reported in the remainder of this article. The dependence of the phoretic mobility on the strength and range of the solute–colloid interactions, solute density and the size of the colloidal particle is presented, which can hardly be quantitatively determined with mesoscopic models. Note that the long-range coulombic interactions are not taken into account, so the simulated system is to measure the diffusio-phoresis of a colloidal particle in the gradient of neutral solutes. The manuscript is organised as follows: the next section introduces the model and simulation methods. Simulation results and discussions are then presented. The last section is the summary.

2. Simulation method

2.1. Model

Molecular dynamics (MD) is implemented to simulate the diffusio-phoresis. All MD simulations are carried out in LAMMPS [49]. The fluid particle i of type α (solvent) or β (solute) interacts with another fluid particle j through the Lennard-Jones (LJ) 12–6 potential that is truncated and shifted at $r_{ij}^t = 4.0$:

$$U_{ij}^{LJ}(r_{ij}) = 4\epsilon_{ij} \left[\left(\frac{\sigma_{ij}}{r_{ij}} \right)^{12} - \left(\frac{\sigma_{ij}}{r_{ij}} \right)^6 \right],$$

$$U_{ij}(r_{ij}) = \begin{cases} U_{ij}^{LJ}(r_{ij}) - U_{ij}^{LJ}(r_{ij}^t) & \text{for } r_{ij} < r_{ij}^t, \\ 0 & \text{for } r_{ij} \geq r_{ij}^t, \end{cases} \quad (1)$$

with ϵ_{ij} and σ_{ij} the LJ constants. Here and in what follows, I use reduced units, based on $\epsilon_{\alpha\alpha}$, $\sigma_{\alpha\alpha}$ and m_α (mass of the solvent particle).

Morse potential is used to model the interactions between the colloid c and fluid particle i of type α or β :

$$U_{ic}^M(r_{ic}) = \epsilon_{ic} \left[e^{-2(r_{ic}-\sigma_{ic})/\kappa_{ic}} - 2e^{-(r_{ic}-\sigma_{ic})/\kappa_{ic}} \right],$$

$$U_{ic}(r_{ic}) = \begin{cases} U_{ic}^M(r_{ic}) - U_{ic}^M(r_{ic}^t) & \text{for } r_{ic} < r_{ic}^t, \\ 0 & \text{for } r_{ic} \geq r_{ic}^t, \end{cases} \quad (2)$$

where ϵ_{ic} , κ_{ic} , and σ_{ic} , respectively, control the interaction strength, interaction range, and the position of the minimum. Note that the subscript c denotes the fixed colloid, and the potential is truncated and shifted at $r_{ic}^t = 7.0$. See Table 1 for the full list of interaction parameters used in this paper (unless otherwise specified).

The concentration gradient can be explicitly simulated by a source and sink region with the fixed number density of solute [48] in a $50.00 \times 19.73 \times h$ box with periodic

Table 1. Table of parameters for interactions between different particles (unless specified).

Lennard-Jones $i-j$	ϵ_{ij}	σ_{ij}	–	r_{ij}^t
solvent–solvent $\alpha - \alpha$	1.0	1.0	–	4.0
solvent–solute $\alpha - \beta$	1.0	1.0	–	4.0
solute–solute $\beta - \beta$	1.0	1.0	–	4.0
Morse i -colloid	ϵ_{ic}	σ_{ic}	κ_{ic}	r_{ic}^t
solvent–colloid $\alpha - c$	1.0	3.0	0.5	7.0
solute–colloid $\beta - c$	$\epsilon_{\beta c}$	3.0	0.5	7.0

boundary conditions, as shown in Figure 1(a). The box height h in the z -direction is varied to keep the pressure at constant. The flow rate of the fluid is measured, whilst keeping the colloid fixed at the origin.

As shown in Figure 1(b), the concentration gradient can also be represented implicitly [45,48] by applying (different) gradient forces f_i on the solvent and solute particles:

$$f_i = \left(\frac{-\partial \mu_i^{\text{bulk}}}{\partial \rho_i} \right)_P \cdot \nabla \rho_i, \quad (3)$$

where μ_i^{bulk} is the chemical potential and ρ_i the number density. The system dimensions are $19.73 \times 19.73 \times h$, and the colloid is fixed at the origin, providing the counteracting force $F_c = -(f_\alpha N_\alpha + f_\beta N_\beta)$ to ensure that there is no net force on the fluid. In the remainder of this paper, model with implicit gradient is used unless otherwise specified (due to its better accuracy and efficiency).

2.2. Simulation details

All simulations are performed in NPT ensemble, with fixed pressure at $P = 0.012$, and temperature at $T = 0.845$. The number of particles is fixed at $N = 12308$ and $N = 7124$ for the system with explicit and implicit gradient, respectively. Nosé–Hoover thermostat with damping constant for temperature $100dt$ and Nosé–Hoover barostat with damping constant for pressure $1000dt$ are implemented, with $dt = 0.001$ representing the length of the time step. As it may be useful to compare simulations with experimental results, in Table 2 quantities in reduced units used in this work are converted into real units. For all real units, the mass and LJ parameters of solvent particles are chosen as those of argon atom.

All initial configurations are prepared as follows. First, $N-1$ solvent particles are uniformly distributed on FCC crystal lattice at low densities to prevent overlap. $N_\beta = \rho_\beta V$ random solvent particles are then replaced with solute particles, where V is the volume of the simulation box and ρ_β is the density of solute. The system is then compressed in z -direction and quenched to the desired pressure. At $\epsilon_{\beta c} = 2.6$, The typical height of the

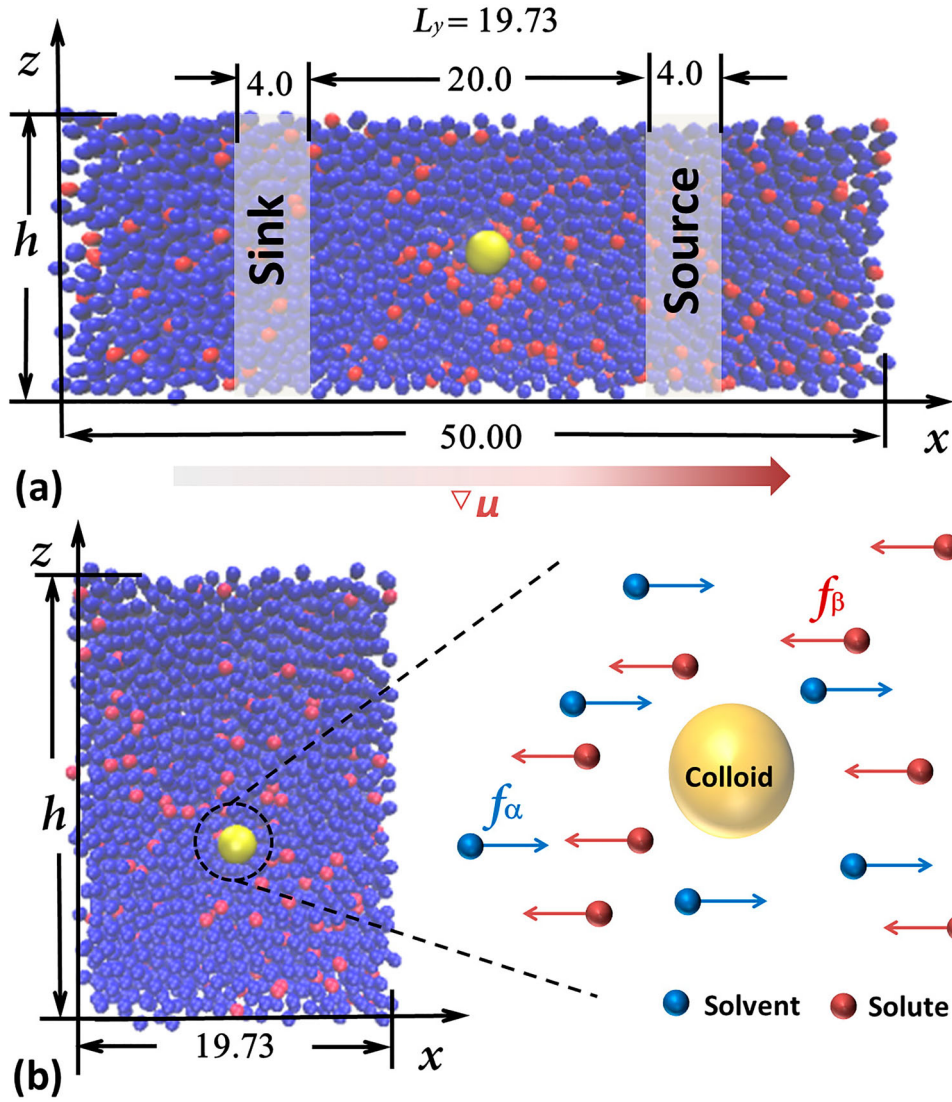


Figure 1. Slice snapshot of the model systems with (a) explicit or (b) implicit concentration gradient of solutes.

Table 2. Comparison of quantities measured in reduced and real units (in terms of argon atom).

Quantities	In reduced unit	In real unit
$\sigma_{\alpha\alpha}$	1.0	0.341 nm
$\epsilon_{\alpha\alpha}$	1.0	10.30 meV
m_{α}	1.0	39.95 g/mol
dt	0.001	2.164 fs
P	0.012	0.5 MPa
T	0.845	101 K

box is $h = 23.92$ for simulations with implicit gradient, and $h = 16.34$ for explicit gradient.

For simulations with explicit concentration gradient, the identities of the fluid particles within the source ($\rho_{\beta} = 0.07$) or sink ($\rho_{\beta} = 0.03$) regions are reset every 5×10^2 simulation steps to maintain a constant gradient and $\rho_{\beta} \sim 0.05$ at $x = 0$. For simulations with an implicit concentration gradient, the identities of solvent and solute particles in the bulk (i.e. far away from the

colloidal particle) are allowed to interchange every 500 simulation steps to keep the density of solute in bulk ρ_{β}^{bulk} constant for at least 4×10^7 simulation steps. Gradient forces f_i along the x -direction are then applied to the solvent and solute particles. Subsequently, a long run (at least 2×10^8 steps) is performed to obtain the flow rate, density profile, etc., which are collected by averaging over 10^5 output configurations separated by 10^3 simulation steps. For both cases, a solute concentration gradient of $|\nabla \rho_{\beta}| = 0.002$ is generated.

Based on the Green–Kubo formula, I determine the radial auto-correlation for the shear terms of stress tensor, $\xi(r)$, which is written as

$$\xi(r) = \frac{V}{k_B T} \int_0^{\infty} [\langle p_{xy}(0, r) p_{xy}(t, r) \rangle + \langle p_{xz}(0, r) p_{xz}(t, r) \rangle + \langle p_{yz}(0, r) p_{yz}(t, r) \rangle] / 3 dt, \quad (4)$$

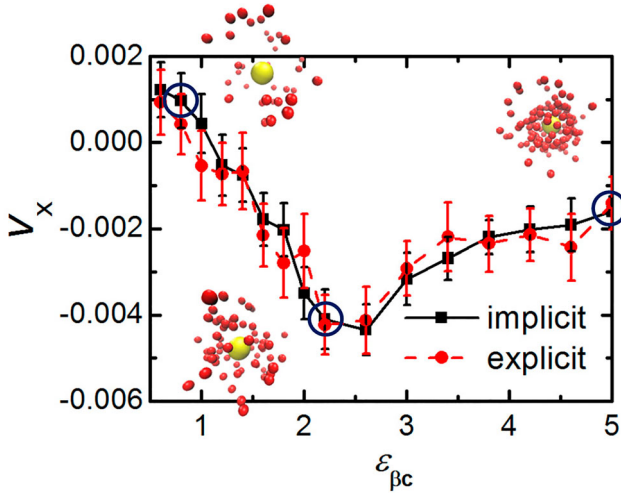


Figure 2. The dependence of velocity of fluids in x -direction, v_x , on the interaction strength between solute and colloid, $\epsilon_{\beta c}$, obtained from simulations with implicit and explicit gradient. The density of solute in bulk is fixed at $\rho_{\beta}^{bulk} = 0.05$. Typical simulation snapshots of solutes around the colloid at $\epsilon_{\beta c} = 0.8$, $\epsilon_{\beta c} = 2.2$ and $\epsilon_{\beta c} = 5.0$ are presented.

where $p_{xy}(t, r)$, $p_{xz}(t, r)$ and $p_{yz}(t, r)$ are off-diagonal stress tensors averaged over particles at a distance r to the fixed colloid, and k_B is the Boltzmann constant.

3. Result and discussion

3.1. Interaction

Figure 2 shows that for all values of $\epsilon_{\beta c}$, the interaction strength between solute and colloid, v_x , the velocity in the direction of phoretic motion obtained from simulations with imposed gradient forces agrees well with that obtained using an explicit concentration source and sink. It is found that v_x depends non-monotonically on $\epsilon_{\beta c}$. For $\epsilon_{\beta c} < 2.5$, the magnitude of v_x increases with $\epsilon_{\beta c}$. This is because the number of adsorbed solute particles, and hence total gradient force exerted on them, increases with $\epsilon_{\beta c}$. If the density profile around the colloid is radially symmetric, the net force density equals $F_x(r) = \rho_{\alpha}(r)f_{\alpha} - \rho_{\beta}(r)f_{\beta}$ and $f_{\alpha}/f_{\beta} = \rho_{\beta}^{bulk}/\rho_{\alpha}^{bulk}$. In that case, an excess of solute (β) would imply $F_x(r) < 0$ and an excess of solvent, $F_x(r) > 0$. The maximum velocity ($v_x^m = -0.004$) is obtained for $\epsilon_{\beta c} \approx 2.5$. When the solute-colloid interaction is further increased, the magnitude of v_x decreases and reaches $v_x \sim -0.002$ at $\epsilon_{\beta c} = 5.0$. This is because a sticky shell of solute particles is effectively trapped around the colloid for larger values of $\epsilon_{\beta c}$, which does not contribute to diffusio-phoresis. The formation of the shell-region is demonstrated by the typical simulation snapshots of solutes around the colloid at $\epsilon_{\beta c} = 0.8$, $\epsilon_{\beta c} = 2.2$ and $\epsilon_{\beta c} = 5.0$ shown in Figure 2.

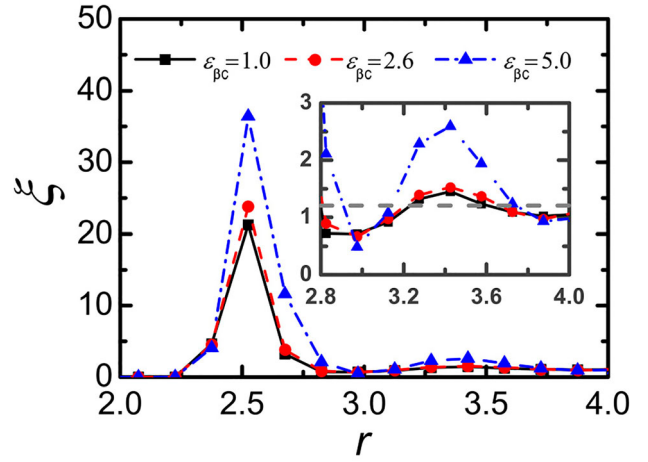


Figure 3. The auto-correlation for the shear terms of stress tensor, ξ , as a function of distance to the colloid, r , at three different $\epsilon_{\beta c}$. The inset magnifies $2.8 < r < 4.0$ part, with grey dashed line indicating the viscosity for system consists of pure LJ particles of $\sigma = 1.0$ and $\epsilon = 1.0$ at the same thermodynamic state.

To validate the existence of shell-region, Figure 3 presents the dependence of auto-correlation for the shear terms of stress tensor ξ as a function of distance to the colloid r , which reflects the local viscosity of the fluid. While $\xi(r)$ is barely changed when $\epsilon_{\beta c}$ is increased from 1.0 to 2.6, its peak around $r \sim 2.5$ mounts up when $\epsilon_{\beta c}$ is increased to 5.0. The peak is generated by the bound particles (mainly solvent), caged by the solute shell formed around $r \sim 3.0$, which is consistent with the position of the first peak of $F_x(r)$ in Figure S2 shown in SI. The magnified inset of Figure 3 presents the secondary peak around $r \sim 3.4$, at which the magnitude of ξ for $\epsilon_{\beta c} = 5.0$ is still larger than the other two cases. This peak is generated by the aggregation of solute particles adsorbed to the shell, constrained by the solute-colloid attraction, in accord with the peak of F_x at the same position. For $r > 4.0$, the value of $\xi(r)$ fluctuates around 1.21, i.e. the viscosity of pure LJ particles at same thermodynamic state obtained by the same method (Equation (4)), indicated by the grey dashed line within inset.

The results obtained here by simulation deviate from the continuum approximation [29,47], for which the magnitude of v_x is determined by

$$v_x = \frac{2\sigma_c T}{9\eta} \int_{\sigma_c}^{\infty} \left[\left(\frac{\sigma_c}{2r} \right) - \left(\frac{3r}{2\sigma_c} \right) + \left(\frac{r}{\sigma_c} \right)^2 \right] A_1(r) \frac{dU_{\beta}(r)}{dr} dr, \quad (5)$$

where σ_c is the radius of colloid, η the viscosity, $A_1(r)$ the asymptotic expression for the first Legendre coefficient and $U_{\beta}(r)$ the solute-colloid interaction. Because

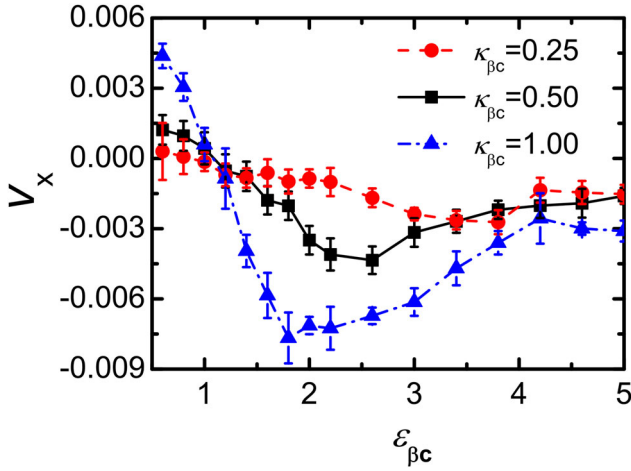


Figure 4. The dependence of the diffusio-phoretic flow velocity v_x on $\epsilon_{\beta c}$, for different values of the range $\kappa_{\beta c}$ of the solute–colloid interaction.

the formation of shell-region is not taken into account, v_x depends linearly on $\epsilon_{\beta c}$ according to Equation (5). See Figures S1–S4 of SI for more results and discussions on the effect of $\epsilon_{\beta c}$ on the diffusio-phoretic motion of colloid.

The magnitude of the phoretic flow also depends on the interaction range. Figure 4 shows the relation between v_x and $\epsilon_{\beta c}$ for various values of $\kappa_{\beta c}$, the range parameter of the solute–colloid interaction. As is to be expected, the magnitude of v_x is larger for larger $\kappa_{\beta c}$ (i.e. larger interactive width), as more solute particles would get attracted within the interface for larger $\kappa_{\beta c}$, a longer range of attraction results in a larger number of adsorbed solute particles. The maximum velocity v_x^m is reached at smaller $\epsilon_{\beta c}$ for larger $\kappa_{\beta c}$.

The dependence of v_x on solvent–colloid interactions is discussed in Figure S6 in SI.

3.2. Density of solute

Figure 5(a) shows the dependence of v_x on $\epsilon_{\beta c}$, at different solute density in bulk, namely $\rho_{\beta}^{bulk} = 0.05$, $\rho_{\beta}^{bulk} = 0.25$ and $\rho_{\beta}^{bulk} = 0.50$. Correspondingly, the number fraction of solutes in bulk are $\phi_{\beta}^{bulk} = 0.066$, $\phi_{\beta}^{bulk} = 0.328$ and $\phi_{\beta}^{bulk} = 0.655$. For $\epsilon_{\beta c} < 2.0$ and $\epsilon_{\beta c} > 4.0$, the value of $v_x(\epsilon_{\beta c})$ barely depends on ρ_{β}^{bulk} . For $2.0 < \epsilon_{\beta c} < 4.0$, the magnitude of v_x is markedly larger for $\rho_{\beta}^{bulk} = 0.05$. When $\rho_{\beta}^{bulk} > 0.25$, the flow velocity saturates at around $v_x = -0.002$ for $\epsilon_{\beta c} > 2.0$. The weaker diffusio-phoresis for larger bulk density of solutes is due to two factors, both related to the fact that the diffusio-phoretic velocity v_x is equal to the product of the gradient of the chemical potential of the solute $\partial\mu_{\beta}^{bulk}/\partial x$ and the excess density of solute in the adsorption layer around the

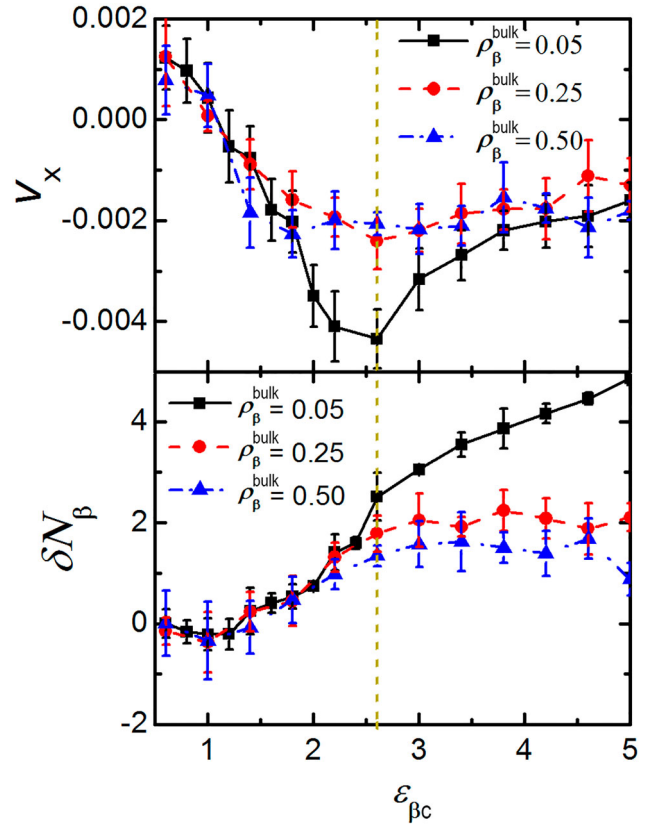


Figure 5. (a) The dependence of diffusio-phoretic flow velocity v_x , on the interaction strength between solute and colloid, $\epsilon_{\beta c}$, for different solute densities ρ_{β}^{bulk} . (b) Number difference of solute particles of left ($x < 0$) and right ($x > 0$) part of the system δN_{β} as a function of $\epsilon_{\beta c}$ at different ρ_{β}^{bulk} . The dashed line indicates $\epsilon_{\beta c} = 2.6$ at which the magnitude of v_x reaches maximum.

colloid [50]

$$v_x = \frac{1}{\eta} \frac{\partial\mu_{\beta}^{bulk}}{\partial x} \int_{\sigma_c}^{\infty} r [\rho_{\beta}(r) - \rho_{\beta}^{bulk}] dr, \quad (6)$$

where $\rho_{\beta}(r)$ and ρ_{β}^{bulk} , respectively, denote the solute density at distance r to the fixed colloid and in bulk region. As solvent and solute form an ideal mixture, this gradient is simply $\nabla\rho_{\beta}/\rho_{\beta}^{bulk}$, which at constant $\nabla\rho_{\beta}$ is inversely proportional to ρ_{β}^{bulk} . The second reason is that the excess of solute in the adsorption layer $\rho_{\beta}^{ex} = \rho_{\beta}^{local} - \rho_{\beta}^{bulk}$ tends to saturate rather quickly with $\epsilon_{\beta c}$. Once that happens, increasing ρ_{β}^{bulk} tends to decrease ρ_{β}^{ex} near the colloid. This effect is counteracted to some extent by the fact that for sufficiently large $\epsilon_{\beta c}$, the total number of adsorbed particles increases.

The increase of ρ_{β}^{bulk} also leads to the decrease of the asymmetric distribution of solutes around the colloid in the presence of the gradient forces. This is illustrated

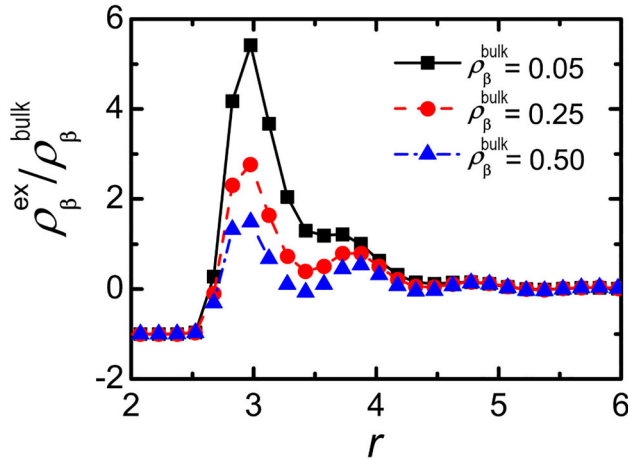


Figure 6. The normalised excess density of solute particles $\rho_{\beta}^{ex}/\rho_{\beta}^{bulk}$ as a function of r at $\epsilon_{\beta c} = 2.6$.

in Figure 5(b). The number difference of solute particles at left ($x < 0$) and right ($x > 0$) part of the system δN_{β} increases obviously with $\epsilon_{\beta c}$ for $\rho_{\beta}^{bulk} = 0.05$. However, for $\rho_{\beta}^{bulk} \geq 0.25$, the value of δN_{β} saturates near $\epsilon_{\beta c} = 2.6$, which is also the point where the diffusio-phoretic flow velocity appears to maximise (indicated by the dashed line). The dependence of asymmetry of solutes distribution on r is also discussed in Figure S7 of SI.

Figure 6 shows the saturation at high values of $\epsilon_{\beta c}$ of the normalised excess density of solute particles adsorbed to the colloid. Upon increasing the solute density in bulk ρ_{β}^{bulk} from 0.05 to 0.25, the peak value of $\rho_{\beta}^{ex}(r)$ at $r = 3.0$ clearly decreases. However, upon further increase in ρ_{β}^{bulk} , the excess density of the adsorbed solute is changed very slightly.

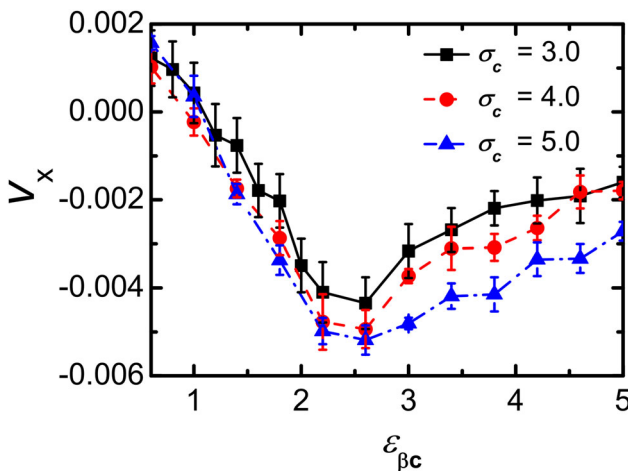


Figure 7. The dependence of velocity in x -direction of fluids, v_x , on the interaction strength between solute and colloid, $\epsilon_{\beta c}$, for different colloid sizes σ_c .

3.3. Size effect

The dependence of v_x on the size of the colloid σ_c , controlled by setting the position of the minimum of the Morse potential as $\sigma_{\alpha c} \equiv \sigma_{\beta c} \equiv \sigma_c$, is shown in Figure 7. Note that the width of the potential well is kept constant, with fixed variations in the truncated cut-off distance and the size of colloid as $\delta r^t = \delta \sigma$. Increasing the size of the colloid increases the magnitude of the diffusio-phoretic flow (for any given $\epsilon_{\beta c}$). Such an effect is to be expected, as the volume of the adsorption region increase with $\sigma_{\beta c}$ and the formation of shell-region depends mainly on $\epsilon_{\beta c}$.

4. Conclusions

To conclude, in this work, how the diffusio-phoretic motion of colloidal particle gets suppressed by the formation of the shell-region is explained numerically. Although the excess density of adsorbed solute increases with the strength of solute–colloid attraction, this effect is counteracted by the fact that very strong binding of the solute suppresses diffusio-phoresis, as the adsorbed layer becomes more viscous. The optimal solute–colloid attraction that maximises the phoretic mobility is thus determined. It is also found that the phoretic motion can be impeded at high solute density in bulk, as both the degree of asymmetric distribution of solutes surrounding the colloid and the excess density of solutes in the adsorption shell decrease with solute density in bulk. The phoretic mobility is also found to depend on interaction range, size and hydrophobicity of the colloid, all of which change the concentration distribution of solutes (or solvents) surrounding the colloid. Similarly, introducing another colloidal particle would also change the magnitude of flow velocity with a perturbation on the concentration field. See Figure S8 in SI for more discussions. The results indicate that diffusio-phoresis may be applied to the selective transport, separation and purification of bio-macromolecules and other types of colloids, due to the sensitive dependence of the diffusio-phoretic mobility on the interaction strength and the density of solutes. However, as the magnitude of flow velocity increases with the solute–colloid interaction range, it might be more efficient to transport bio-macromolecules such as protein or DNA in a concentration gradient of electrolyte with long-range interactions, i.e. by eletro-phoresis.

Acknowledgments

The author appreciates illuminating comments from Prof. Daan Frenkel and fruitful discussions with Yawei Liu, Raman Ganti and Simon Ramirez.

Disclosure statement

No potential conflict of interest was reported by the author.

Funding

This work was supported by National Natural Science Foundations of China [grant number 2016YFA0501601] and National Key Research and Development Program of China [grant number 11602279].

References

- [1] J.C. Eijkel and A. van den Berg, *Chem. Soc. Rev.* **39**, 957 (2010).
- [2] J.L. Anderson and D.C. Prieve, *Sep. Purif. Methods* **13**, 67 (2006).
- [3] O. Annunziata, D. Buzatu and J.G. Albright, *J. Phys. Chem. B* **116**, 12694 (2012).
- [4] J. Deseigne, C. Cottin-Bizonne, A.D. Stroock, L. Bocquet and C. Ybert, *Soft Matter* **10**, 4795 (2014).
- [5] J. Palacci, B. Abecassis, C. Cottin-Bizonne, C. Ybert and L. Bocquet, *Phys. Rev. Lett.* **104**, 138302 (2010).
- [6] J.S. Paustian, C.D. Angulo, R. Nery-Azevedo, N. Shi, A.I. Abdel-Fattah and T.M. Squires, *Langmuir* **31**, 4402 (2015).
- [7] D.C. Prieve, S.M. Malone, A.S. Khair, R.F. Stout and M.Y. Kanj, *Proc. Natl Acad. Sci. USA* **116**, 18257 (2019).
- [8] M. Yang, A. Wysocki and M. Ripoll, *Soft Matter* **10**, 6208 (2014).
- [9] Y. Zhao, C. Zhao, J. He, Y. Zhou and C. Yang, *Soft Matter* **9**, 7726 (2013).
- [10] A. Wurger, *Rep. Progr. Phys.* **73**, 126601 (2010).
- [11] M. Braibanti, D. Vigolo and R. Piazza, *Phys. Rev. Lett.* **100**, 108303 (2008).
- [12] J. Burelbach, D. Frenkel, I. Pagonabarraga and E. Eiser, *Eur. Phys. J. E* **41**, 7 (2017).
- [13] J. Burelbach, M. Zupkauskas, R. Lamboll, Y. Lan and E. Eiser, *J. Chem. Phys.* **147**, 094906 (2017).
- [14] L. Fu, S. Merabia and L. Joly, *Phys. Rev. Lett.* **119**, 214501 (2017).
- [15] Y.T. Maeda, A. Buguin and A. Libchaber, *Phys. Rev. Lett.* **107**, 038301 (2011).
- [16] R. Piazza, *Soft Matter* **4**, 1740 (2008).
- [17] R. Piazza and A. Parola, *J. Phys.: Condens. Matter* **20**, 153102 (2008).
- [18] T. Tsuji, K. Kozai, H. Ishino and S. Kawano, *Micro Nano Lett.* **12**, 520 (2017).
- [19] D. Vigolo, R. Rusconi, H.A. Stone and R. Piazza, *Soft Matter* **6**, 3489 (2010).
- [20] D. Vigolo, J. Zhao, S. Handschin, X. Cao, A.J. deMello and R. Mezzenga, *Nat. Sci. Rep.* **7**, 1211 (2017).
- [21] C.J. Wienken, P. Baaske, U. Rothbauer, D. Braun and S. Duhr, *Nat. Commun.* **1**, 100 (2010).
- [22] M. Wolff, J.J. Mittag, T.W. Herling, E.D. Genst, C.M. Dobson, T.P. Knowles, D. Braun and A.K. Buell, *Nat. Sci. Rep.* **6**, 22829 (2016).
- [23] T.Y. Molotilin, V. Lobaskin and O.I. Vinogradova, *J. Chem. Phys.* **145**, 244704 (2016).
- [24] I. Semenov, S. Raafatnia, M. Sega, V. Lobaskin, C. Holm and F. Kremer, *Phys. Rev. E* **87**, 022302 (2013).
- [25] R.F. Stout and A.S. Khair, *Phys. Rev. Fluids* **2**, 014201 (2017).
- [26] M. Tanaka and A.Y. Grosberg, *Eur. Phys. J. E* **7**, 371 (2002).
- [27] M. Tanaka, *Phys. Rev. E* **68**, 061501 (2003).
- [28] K.L. Saar, Y. Zhang, T. Muller, C.P. Kumar, S. Devenish, A. Lynn, U. Lapinska, X. Yang, S. Linse and T.P.J. Knowles, *Lab Chip* **18**, 162 (2017).
- [29] J.L. Anderson, *J. Colloid Interface Sci.* **82**, 248 (1981).
- [30] A.S. Khair, *J. Fluid. Mech.* **731**, 64 (2013).
- [31] R.P. Sear and P.B. Warren, *Phys. Rev. E* **96**, 062602 (2017).
- [32] D. Velegol, A. Garg, R. Guha, A. Kar and M. Kumar, *Soft Matter* **12**, 4686 (2016).
- [33] B. Abecassis, C. Cottin-Bizonne, C. Ybert, A. Ajdari and L. Bocquet, *Nat. Mater.* **7**, 785 (2008).
- [34] J.T. Ault, P.B. Warren, S. Shin and H.A. Stone, *Soft Matter* **13**, 9015 (2017).
- [35] J.T. Ault, S. Shin and H.A. Stone, *J. Fluid. Mech.* **854**, 420 (2018).
- [36] S. Shin, J.T. Ault, P.B. Warren and H.A. Stone, *Phys. Rev. X* **7**, 041038 (2017).
- [37] S. Shin, E. Um, B. Sabass, J.T. Ault, M. Rahimi, P.B. Warren and H.A. Stone, *Proc. Natl Acad. Sci. USA* **113**, 257 (2016).
- [38] A. Banerjee, I. Williams, R.N. Azevedo, M.E. Helgeson and T.M. Squires, *Proc. Natl Acad. Sci. USA* **113**, 8612 (2016).
- [39] N. Shi, R. Nery-Azevedo, A.I. Abdel-Fattah and T.M. Squires, *Phys. Rev. Lett.* **117**, 258001 (2016).
- [40] R. Sear, *Phys. Rev. Lett.* **122**, 128101 (2019).
- [41] M. Yang, R. Liu, F. Ye and K. Chen, *Soft Matter* **13**, 647 (2017).
- [42] T. Chen, C. Xu and Z. Ren, *J. Ind. Manag. Optim.* **13**, 1 (2017).
- [43] M.-J. Huang, J. Schofield and R. Kapral, *Soft Matter* **12**, 5581 (2016).
- [44] Y. Liu, R. Ganti and D. Frenkel, *J. Phys.: Condens. Matter* **30**, 205002 (2018).
- [45] H. Yoshida, S. Marbach and L. Bocquet, *J. Chem. Phys.* **146**, 194702 (2017).
- [46] R. Ganti, Y. Liu and D. Frenkel, *Phys. Rev. Lett.* **119**, 038002 (2017).
- [47] N. Sharifi-Mood, J. Koplik and C. Maldarelli, *Phys. Rev. Lett.* **111**, 184501 (2013).
- [48] Y. Liu, R. Ganti, H.G. Burton, X. Zhang, W. Wang and D. Frenkel, *Phys. Rev. Lett.* **119**, 224502 (2017).
- [49] S. Plimpton, *J. Comput. Phys.* **117**, 1 (1995).
- [50] J.L. Anderson, M.E. Lowell and D.C. Prieve, *J. Fluid Mech.* **117**, 107 (1982).